

pubs.acs.org/JACS Article

Imidacloprid Crystal Polymorphs for Disease Vector Control and Pollinator Protection

Xiaolong Zhu, Chunhua T. Hu, Bryan Erriah, Leslie Vogt-Maranto, Jingxiang Yang, Yongfan Yang, Mengdi Qiu, Noalle Fellah, Mark E. Tuckerman, Michael D. Ward,* and Bart Kahr*



Cite This: J. Am. Chem. Soc. 2021, 143, 17144–17152



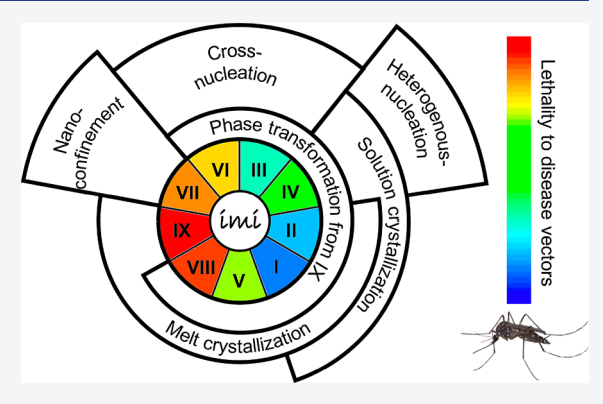
ACCESS

III Metrics & More

Article Recommendations

Supporting Information

ABSTRACT: Imidacloprid, the world's leading insecticide, has been approved recently for controlling infectious disease vectors; yet, in agricultural settings, it has been implicated in the frightening decline of pollinators. This argues for strategies that sharply reduce the environmental impact of imidacloprid. When used as a contact insecticide, the effectiveness of imidacloprid relies on physical contact between its crystal surfaces and insect tarsi. Herein, seven new imidacloprid crystal polymorphs are reported, adding to two known forms. Anticipating that insect uptake of imidacloprid molecules would depend on the respective free energies of crystal polymorph surfaces, measurements of insect knockdown times for the metastable crystal forms were as much as nine times faster acting than the commercial form against *Aedes, Anopheles,* and *Culex* mosquitoes as well as *Drosophila* (fruit flies). These results suggest



that replacement of commercially available imidacloprid crystals (a.k.a. Form I) in space-spraying with any one of three new polymorphs, Forms IV, VI, IX, would suppress vector-borne disease transmission while reducing environmental exposure and harm to nontarget organisms.

■ INTRODUCTION

Insecticides are frequently harmful to nontarget organisms and their accumulation in the environment is inconsistent with the United Nations roadmap to a sustainable world by 2030. Meanwhile, the achievement of sustainable development goals (SDG) such as "zero hunger" and "good health and well-being" is linked to the control of pests, paradoxically by using chemical insecticides. The neonicotinoid class of insecticides is increasingly used for controlling infectious disease vectors² as a response to the widespread resistance of vectors to pyrethroids,3 mainstays of public health officials since the 1970s.4 In recent years, the World Health Organization (WHO) introduced two neonicotinoid insecticides, imidacloprid (IMI; 1-[(6-chloro-3-pyridinyl)-methyl]-N-nitro-2-imidazolidinimine; Figure 1) and clothianidin, for the control⁵ of dengue fever and malaria, which afflict 390⁶ and 200⁷ million humans per year, respectively. IMI is now used in indoor and outdoor space sprays to control the Aedes mosquito,8 a vector for dengue, chikungunya, yellow fever, and Zika virus.⁷ IMI also has the potential to control Anopheles and Culex mosquitoes, vectors for malaria and lymphatic filariasis, respectively. In space spray applications, IMI functions as a contact insecticide wherein insects absorb the toxicant molecules through the direct contact of tarsi with the surfaces of IMI microcrystals. 10,11 Once absorbed and transported through the hemolymph, IMI binds to nicotinic acetylcholine

receptors (nAChRs) in the central nervous system, a unique mode of action for insecticides. 12

High insecticidal potency and low mammalian toxicity 12 have ensured the popularity of IMI (the world's leading insecticide), ¹³ with registrations in more than 120 countries. ¹ As a foliar spray, in which IMI controls phytophagous agricultural pests systemically as well as through contact, 10,11 IMI has contaminated soil is as well as surface and underground water,16 and it threatens the survival17 and reproduction¹⁸ of birds. Moreover, the extensive use of IMI in agriculture appears to be connected to a decrease in insect biomass^{19,20} and especially worrying declines in bee colonies,^{21–24} known as colony collapse disorder (CCD). The science of CCD is complex. Mites and viruses, in addition to neonicotinoids, have been implicated pollinator declines, but even sublethal exposures of IMI and other neonicotinoids, through systemic contamination of plants, likely compromise colony viability by affecting the diversity of the food supply or bee immune health, or both.²⁵

Received: July 24, 2021 Published: October 12, 2021





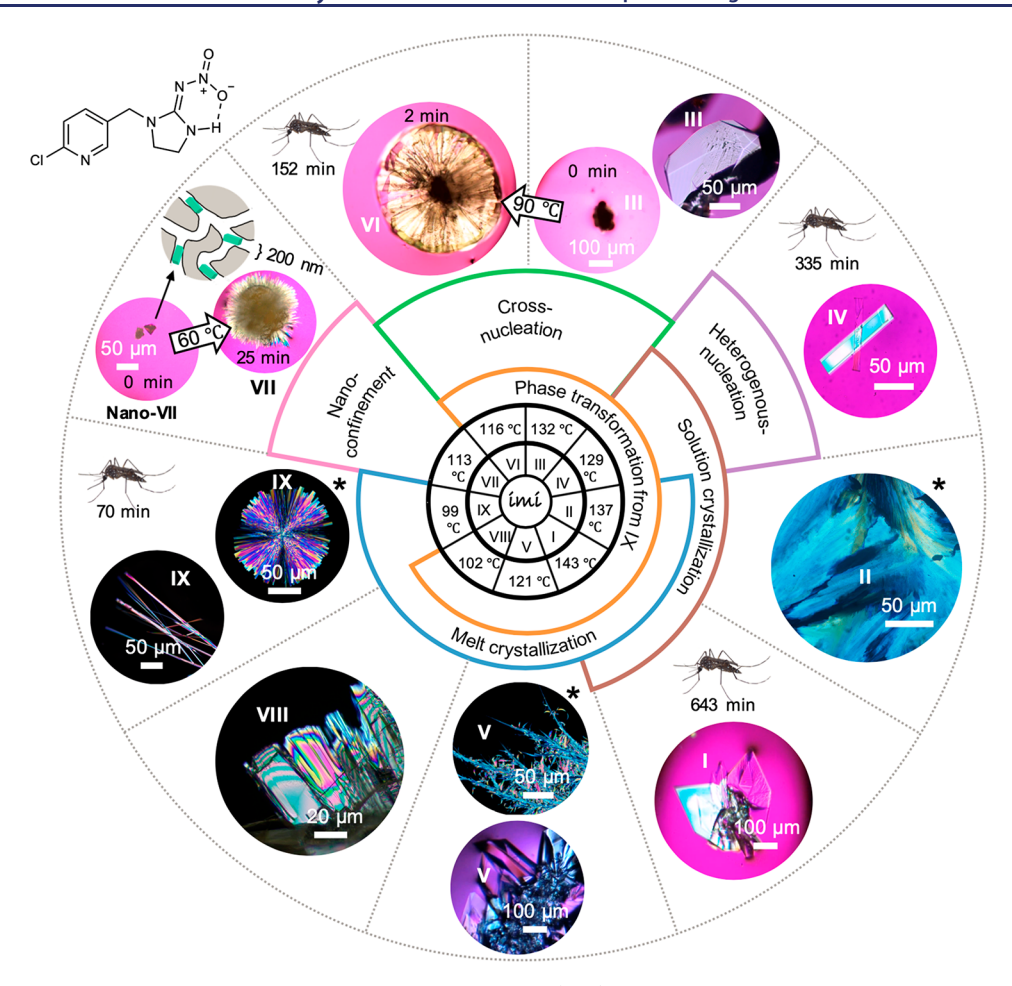


Figure 1. Imidacloprid polymorphism. Molecular structure of imidacloprid (IMI) is shown on the upper left corner. The melting points and crystallization methods are labeled next to each polymorph. Polarized-light optical micrographs of samples confined between glass slides are labeled with *, which include spherulites of Form IX, chaotic textures of Form V, and flat crystalline domains of Form II grown from the melt at ambient temperature. Single crystals of Forms I, III, IV, and V grown from melt in the presence of respective crystal seeds were prepared on a microscope hot stage at 135, 130, 126, and 120 °C, respectively. Form VI was obtained through cross-nucleation on Form III in the melt at 90 °C. Form VII was obtained by seeding nano-Form VII confined in controlled pore (200 nm) glass into the melt at 60 °C. Single crystals of Forms VIII and IX grown from melt at 85 and 70 °C, respectively. Polymorphs with *Aedes* mosquitos are selected for lethality measurements. The median knockdown times (KT_{50}) for female *Aedes* are given in minutes.

France has adopted the precautionary principle and banned IMI and four other neonicotinoids²⁶ out of concern that CCD threatens the global food supply. The United States has not been as aggressive as the European Union in restricting neonicotinoids. As uncertainties about the science linger, companies may continue to market IMI. This argues for science-based strategies that enhance IMI contact activity while reducing the amount used, with concomitant reductions in its exposure to nontarget organisms. Herein, we demonstrate that new crystal polymorphs (a.k.a. Forms) of IMI can be more effective and used in reduced amounts, consistent with integrated pest management (IPM) strategies.²⁷

The efficacy of IMI applications, such as outdoor residual spraying for vector control, ²⁸ depends upon the uptake of IMI by the insect when contacting the crystal surfaces. The speed of contact activity of IMI is regarded as slow, however. ² This characteristic enables the survival of pests and vectors after contact with IMI crystals, leading to continued crop damage and disease transmission, respectively, as well as the development of resistance. We previously illustrated that the activity of organochlorine, ^{29,30} organofluorine, ³¹ and pyrethroid insecti-

cides³² can be increased substantially with metastable crystal forms, capitalizing on higher crystal free energies to surrender surface toxicant molecules more readily to insect tarsi upon contact. Herein, we describe the discovery of seven new IMI polymorphs that are more lethal than the common Form I found in commercial formulations. Insect lethality assays of these polymorphs, prepared easily by cooling melts or from solution, and spanning a range of metastabilities, reveal that some of the new forms act much more rapidly than Form I against the common fruit fly Drosophila and the disease vectors Aedes, Anopheles and Culex mosquitoes. Moreover, the new polymorphs exhibit kinetic stability (persistence) at ambient temperatures, promising improved effectiveness of IMI in a variety of formulations. The results here illustrate that control of IMI polymorphism may be a sustainable strategy for improving its contact efficacy while reducing the quantity of IMI required, providing a pathway to delay the onset of resistance and minimize environmental and ecological impact.

■ RESULTS AND DISCUSSION

New Polymorphs of Imidacloprid. Despite the considerable study and wide use of IMI as a contact insecticide, only

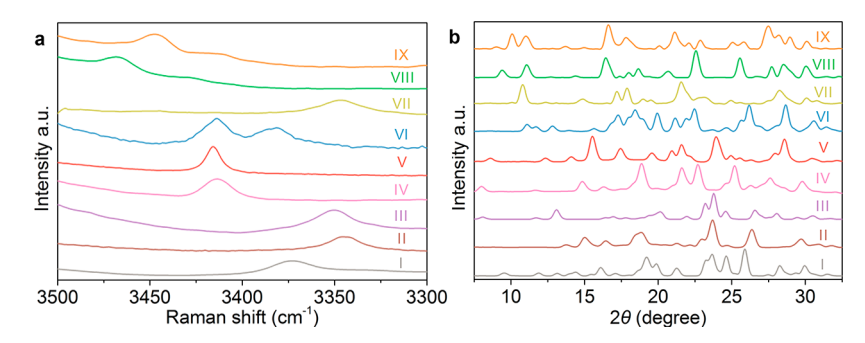


Figure 2. Spectroscopic characterization. (a) Raman spectra revealing the N-H stretch in IMI polymorphs. (b) Powder X-day diffraction patterns of IMI polymorphs. Powders were loaded into a Kapton capillary.

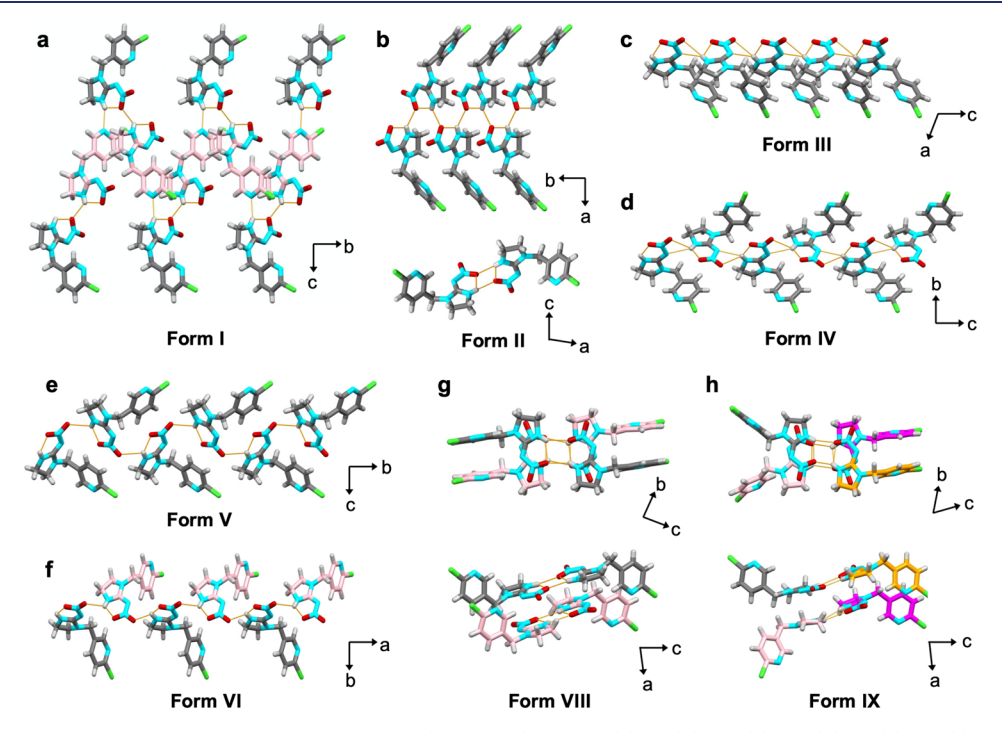


Figure 3. Intermolecular packing motifs in the IMI polymorphs. (Parts a—h) Form I (a), II (b), III (c), IV (d), V (e), VI (f), VIII (g), and IX (h). Atom color: carbon (gray, pink, orange, and magenta for crystallographically independent molecules, respectively); hydrogen (light gray); oxygen (red); nitrogen (cyan); chlorine (green). Hydrogen bonds are represented by orange dash lines.

two crystal structures have been determined, both measured at ambient temperature and designated as Form I^{33,34} and Form II. 35,36 Solution crystallization of IMI from a variety of organic solvents produced Form I, while Form II and a new polymorph, Form IV, can be obtained from acetone and ethanol solutions, respectively (SI, Table S1). Melt crystallization 32,38,39 resulted in the formation of other new polymorphs. Commercial IMI (Sigma-Aldrich) Form I confined between glass slides was melted at ca. 180 °C, above its melting point $(T_m(Form I) = 143 \, ^{\circ}C)$ on a microscope hot stage. The melt subsequently was allowed to cool to ambient temperature (25 °C), resulting in the emergence of polycrystalline spherulites, 40 composed of twisted^{41,42} needles, after 1 week (Figure 1). Micro-Raman spectroscopy (of the N-H stretching region) and powder Xray diffraction (PXRD) confirmed that the spherulites were a new polymorph, herein designated as Form IX (Figure 2; SI, Figures S1-S3). On rare occasions, chaotic polycrystalline fibrils of a new polymorph, Form V (Figure 1), and flat crystalline domains of Form II (Figure 1), also crystallized from the melt. The polymorphs were designated according to

their melting points, which were measured visually on the microscope hot stage.

The complete crystallization of IMI melt confined between glass slides required roughly one month at 25 °C due to its nearby glass transition temperature at $T_g = 15$ °C (SI, Figure S4). Crystallization could be accelerated, however, by removal of the upper cover slide after the melt was cooled. Form IX needles emerged from the melt droplets on uncovered glass slides after 2 days at ambient temperature, continuing to grow for 1 week. Form IX is stable in open air for up to six months at ambient temperature, although on rare occasions, Form IX crystals transformed after one month to other polymorphs, which micro-Raman and PXRD revealed were the known Forms I and II as well as five new polymorphs, herein designated as Forms III, IV, V, VI, and VIII (Figure 2; SI, Figure S1 and S2). Alternatively, Form IV could be prepared through heterogeneous nucleation by introducing a seed crystal of commercial clothianidin ($T_m = 179$ °C), another leading neonicotinoid insecticide, to the IMI melt at 60-100 °C (SI, Figure S5). Curiously, seeding of melts with Form III crystals at 70-100 °C afforded selective cross-nucleation 43-45

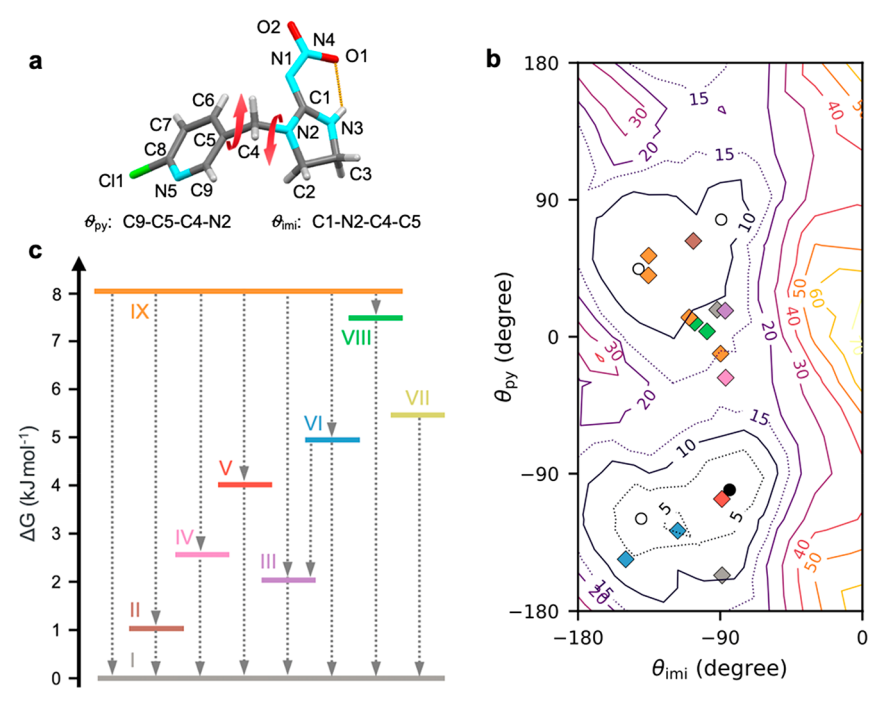


Figure 4. Conformational analysis and thermodynamic stabilities of IMI polymorphs. (a) Torsional angles are indicated by θ_{py} and θ_{imi} . (b) Relative energy (kJ mol⁻¹) as a function of the torsional angles for the IMI molecule based on constrained DFT optimizations. The conformers present in the IMI polymorphs (colored diamonds) are not always near the global minimum (black circle) or local minima (white circles)). Intermediate low-energy contours are shown as dotted lines to highlight the energy basins near the local minima. (c) Summary of phase transformations among IMI polymorphs at and above ambient temperature. Arrows correspond to transformations via motion of an interface after nucleation of a new phase was detected. Polymorph free energies relative to Form I were estimated from $\Delta G = (T_{m(I)} - T_m)\Delta H/T_{m(I)}$, where $T_{m(I)}$ is the melting point of Form I, T_m the melting points of the various crystal forms, and $\Delta H = 28.12$ kJ mol⁻¹, the heat of fusion measured for Form I.

of another new polymorph, herein designated as Form VI (Figure 1; SI, Table S2). Form III could in turn be obtained by cross-nucleation on Form VI at ambient temperature (SI, Figure S6). Nanoconfinement of the IMI melt in controlled pore glass beads⁴⁶ (CPG, pore size = 35, 100, or 200 nm) at ambient temperature produced another new polymorph, Form VII, which was not observed in bulk crystallizations. The Raman spectroscopy and PXRD data confirmed that the confined Form VII was distinct from all other IMI polymorphs. Form VII confined within CPG beads was stable for at least one month at ambient temperature, eventually transforming to Form I. Addition of the CPG beads containing seeds of Form VII to an IMI melt at 60 °C nucleated large needles of Form VII (Figure 1) that grew free from the glass. The needles were identified by Raman spectroscopy as the same phase as the nanoscopic particles in the glass. Rapid cross-nucleation (<10 min.) of Form II on the Form VII needles, however, prevented harvesting of Form VII crystals for single crystal X-ray diffraction analysis (SI, Figure S7). Melt crystallization above 85 °C afforded Form VIII (Figure 1).

Structural and Conformational Analysis of IMI Polymorphs. Seven of the nine IMI polymorphs (Form II was not redetermined and Form VII was not stable) were prepared as single crystals amenable to single-crystal X-ray diffraction at 100 K (SI, Figure S8). Single crystals of IMI polymorphs III, IV, V, VI, VIII, and IX for structure determination were obtained by melt crystallization from seeds (Figure 1; SI, Figure S9). The crystal structure of Form I determined here at 100 K was essentially identical to its structure determined previously at room temperature. All eight polymorphs were refined in the centrosymmetric space groups of $P2_1/c$ (or its nonstandard setting $P2_1/n$) or P1 (SI,

Figure S10 and S11, Table S3). Although the nitroguanidine group in IMI potentially can adopt two tautomeric forms (SI, Figure S12), all the crystal structures contained the tautomer illustrated in Figure 1, featuring a double bond exocyclic to the imidazolidinyl ring with an intramolecular NH···O(nitro) hydrogen bond. The NH hydrogen atoms were located in the difference synthesis. The tautomers were also easily distinguished from the bond lengths of the heavy atoms. One tautomer would have a C1=N1 double bond that would be shorter than its N1-N4 single bond. The other tautomer would have a C1-N1 single bond considerably longer than an N1=N4 double bond. The observed values are consistent with C=N and N-N bonds. Moreover, the planar six membered rings are consistent with an intramolecular N-H-O hydrogen bond with an endocyclic C=N double bond. This observed IMI tautomer has only one hydrogen bond donor (N-H) but four potential acceptors-two nitro group oxygens, the pyridyl nitrogen, and the exocyclic guanidine nitrogen.

The intermolecular hydrogen bonds differ substantially among polymorphs (Figure 3). IMI molecules in Forms I, II, and III are organized as zigzag chains, head-to-head bilayers, and head-to-head columns, respectively. One dimensional intermolecular hydrogen-bonded chains (catemers) adopt a herringbone arrangement in Forms IV, V and VI. Intra- and intermolecular hydrogen bonding between the imidazolidinyl and nitro groups in Forms VIII and IX results in dimers.

The intramolecular $N-H\cdots O$ hydrogen bond in the nitroguanidine group of all eight IMI polymorphs results in a pseudo six-membered ring (Figure 4a), which restricts the conformational freedom about the N^1-N^4 bond. The preference for one tautomer also restricts the N^1-C^1 bond. Therefore, the flexibility primarily arises from the two variable

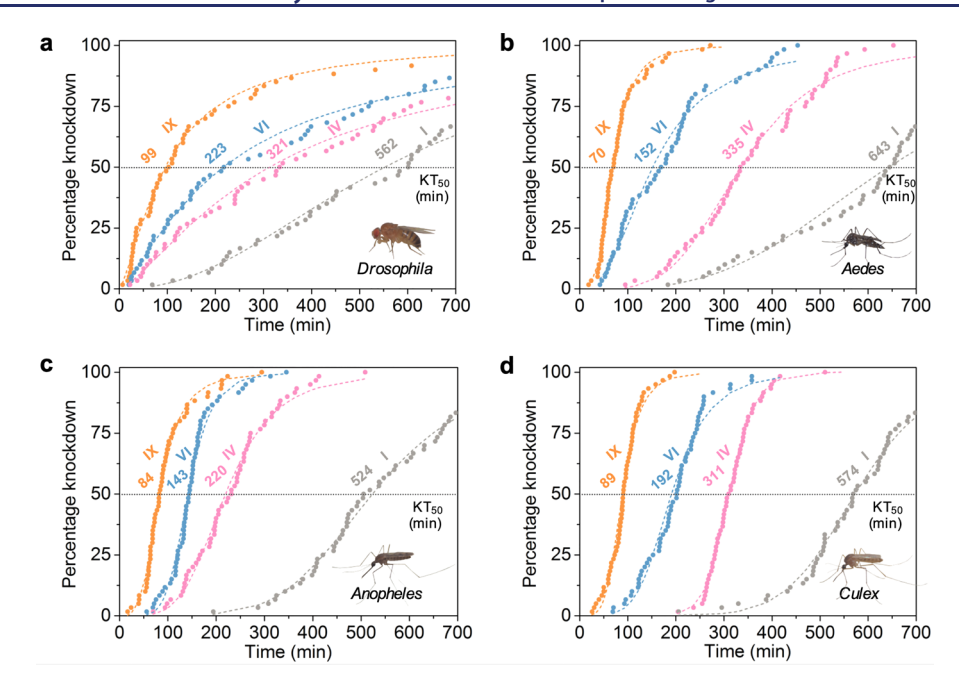


Figure 5. Lethalities of IMI polymorphs against (a) Drosophila melanogaster, (b) Aedes aegypti, (c) Anopheles quadrimaculatus, and (d) Culex quinquefasciatus. Each symbol corresponds to one female. Dashed lines indicate logistic regression of knockdown-time curves. The median knockdown time for each curve is denoted by its intersection with the horizontal KT_{50} marker. Insets: Photographs of typical female mosquitoes.

torsional angles defined by $C^9-C^5-C^4-N^2$ and $C^1-N^2-C^4-C^5$ atom sequences between the pyridyl and the imidazolidinyl rings, herein designated as θ_{py} and θ_{imi} , respectively (Figure 4a; SI, Table S4).

The relative gas phase energies of the IMI conformers in the polymorphs were calculated using density functional theory (DFT) (see Methods), adding six new experimental structures to those reported previously for Form I and II. Conformer energies were determined as a function of $\theta_{\rm py}$ and $\theta_{\rm imi}$ angles (Figure 4b, SI) as previously obtained. The fixed $\theta_{\rm py}$ and $\theta_{\rm imi}$ torsional angles are defined as previously reported; all other degrees of freedom were allowed to relax. The observed conformers are not found near the local minima (except for Form V), with energies that span a range of more than 15 kJ mol $^{-1}$ (Figure 4b).

Thermodynamic Stability and Free Energy Ranking. IMI polymorphs are typically stable for at least 6 months under ambient air and temperature. Although the polymorphic forms were distinguishable by the morphologies and interference colors between crossed polarizers, their identity and any phase transformations were corroborated by micro-Raman spectroscopy and PXRD. Form IX held at 95 °C on a microscope hot stage in air was transformed to Form V in 3 min, which then was converted to Form I at 110 °C in 2 min (SI, Figure S13). Form I also was nucleated directly on the surface of Form IX at T > 70 °C. Form IX crystals grown while confined between glass slides were transformed to Form I, V, or VI at 80 °C within 1 min (SI, Figure S13). Surprisingly, Form IX only occasionally transforms to Forms II, III, or VIII at ambient temperature despite having conformers in the same energetic basin (Figure 4b), suggesting nucleation is frustrated by an energy barrier associated with both intra- and intermolecular changes. Form VI was transformed to III when they were in contact at 110 °C. All Forms II-IX were observed to transform to Form I in some trials upon being heated in a hot stage or differential scanning calorimeter (DSC),

corroborating commercial Form I as the most thermodynamically stable (SI, Figure S4).

The melting points of the polymorphs range from 99 $\leq T_{\rm m} \leq$ 143 °C (Figure 1), reflecting a wide range of crystal free energies (Figure 4c). The free energy ranking discerned from the melting points (I < II < III < IV < V < VI < VII < VIII < IX) is in accord with the ranking deduced from the phase transformation behavior (Figure 4c). This order contrasts with the order of the relative energies of the aforementioned gas phase molecular structures of the IMI conformers observed in the polymorphs (Figure 4b), illustrating that crystal thermodynamic stability rankings in these cases depend less on the molecular conformation than on intermolecular interactions.

Lethality Ranking of IMI Polymorphs. IMI Forms IV, VI, and IX, which span a wide range of free energies (Figures 1 and 4c), were selected for lethality comparisons with the commercial Form I, because these forms were readily prepared from the melt and were kinetically stable against transformations to other polymorphs. Female fruit flies (Drosophila melanogaster), a common pest considered to be a reliable mosquito proxy for insecticide development, ⁴⁹ were exposed in tarsal assays to 2.00 mg of nearly monodisperse (ca. 10 μ m) microcrystals of each IMI polymorph, distributed uniformly on the bottom surfaces of separate 35 mm-diameter polystyrene Petri dishes (SI, Figure S14). Fruit flies exhibited tremors after contacting IMI, followed by prostration, then knockdown.¹³ A video camera was used to record the knockdown times for each insect. KT₅₀ values, the times required for 50% of the insects to become immobile and supine, were calculated by logistic regression (SI, Figure S14). Shorter KT₅₀ values correspond to greater lethality. The KT50 values spanned the range of 562-99 min, decreasing in the order Forms I > IV > VI > IX (Figure 4a; SI, Table S4). Accordingly, Forms IX, VI and IV were 5.7, 2.5, and 1.8 times faster-acting than Form I.

Female Aedes aegypti, Anopheles quadrimaculatus, and Culex quinquefasciatus mosquitoes were approximately 20 times more

susceptible to IMI than *Drosophila*. The knockdown behavior observed for mosquitoes exposed to 0.10 mg of IMI microcrystals paralleled that of *Drosophila* (Figure 5a) but with steeper slopes for the knockdown-time curves (Figure 5b–d; SI, Table S4). KT_{50} values decreased in the order Forms I > IV > VI > IX for all three mosquitoes, with the same ordering observed for the fruit flies. Accordingly, Forms IX, VI, and IV are more than 6, 3, and 2 times faster than Form I for mosquitoes. Notably, the KT_{50} values for *Aedes* exposed to Forms I and IX microcrystals were 643 and 70 min, respectively, a ratio of 9.2.

Aedes and Drosophila exposed to IMI vapor remained viable with no nerve firing symptoms after 12 h (SI, Figure S15), corroborating the reported low vapor pressure and inactive vapor phase of IMI. Therefore, the different lethalities of IMI polymorphs can be attributed to the rate of uptake of molecules from crystal surfaces upon contact with the insect tarsi. The remarkable decrease in knockdown times of metastable polymorphs indicates that the rate-limiting step in the contact exposure of IMI is the detachment of molecules from crystal surfaces, consistent with the correlation of the KT₅₀ values with the crystal free energies (Figures 1 and 4c).

Current gains in infectious disease control are greatly threatened by the widespread resistance to conventional insecticides,³ such as pyrethroids. The recent outbreaks and spread of Zika virus^{51,52} and yellow fever⁵³ transmitted by Aedes mosquitoes also pose new challenges to public health. Meanwhile, mosquito metabolism and population size will increase sharply in many regions as the planet continues to warm,⁵⁴ requiring more effective vector control. Fast action is an important consideration for public health insecticides, as vectors need to be quickly incapacitated to interrupt disease transmission. The efficacy of clothianidin, the other neonicotinoid used as the latest chemical weapon for vector control,5 has been compromised due to the development of resistance. 55 Therefore, improving the efficacy of IMI is critical for mitigating vector resistance to neonictonoids. Previously, we reported simulations which demonstrated that a more active polymorph of deltamethrin could have a substantial impact on malaria-transmitting Anopheles mosquitoes.³² These epidemiological models, however, are not readily translated to Aedes mosquitoes owing to their more complex life cycles and, to our knowledge, the absence of important parameters required for modeling. Nevertheless, the new IMI polymorphs reported here significantly increase the contact activity of IMI, minimizing its knockdown time.² The increased uptake speeds of IMI molecules from metastable polymorphs are expected to quickly saturate overexpressed detoxification enzymes, 56 therefore ensuring that a lethal dose will reach the target site and circumvent nascent insecticide resistance.

CONCLUSIONS

Seven (Forms III—IX) new polymorphs of the world's leading insecticide, imidacloprid (IMI), were discovered, adding to the two previously known forms, one of which is used commercially. The solid-state structures of six of these seven forms (Forms III—VI, VIII, and IX) were determined by single crystal X-ray analysis. The relative stabilities of the nine polymorphs (Forms I—IX) were deduced from melting points and solid-state phase transformations. The contact insecticide efficacy of three of the newly discovered forms were compared with the commercial Form I against *Drosophila* as well as *Anopheles, Aedes*, and *Culex* mosquitoes. The knockdown times

were inversely correlated with the thermodynamic stability ranking of the four polymorphs, consistent with more rapid delivery of the toxicant molecules from less stablecrystal surfaces to the insect tarsi. Notably, Form IX is easy to prepare and its microcrystals are stable against transformation in air for at least six months, suggesting this polymorph is a viable candidate for improved infectious disease control while reducing environmental exposure and associated harm to nontarget organisms.

METHODS SECTION

Crystallization of IMI Polymorphs. Single crystals of IMI Forms II, and IV were prepared in 20 mL glass vials by slow evaporation from saturated acetone and ethanol solutions at ambient temperature, respectively (SI, Table S1). Alternatively, Form IV could be prepared by seeding crystalline clothianidin (the commercial form) to the IMI melts at 60-100 °C. Forms III and V were prepared by phase transformations from Form IX at RT. Single crystals of Form VI were prepared by seeding Form III crystals in melts at 70-100 °C. Form VII was prepared by nanoconfinement of the melts using controlled pore glass (CPG, pore size = 35, 100, or 200 nm) at 180 °C in a DSC, then cooling to ambient temperature. The bulk Form VII was obtained by seeding Form VII confined in CPG to the melt at 60 °C. Forms VIII and IX were prepared by holding the supercooled melt on glass slides at 25-80 and 85 °C, respectively. Single crystals of IMI polymorphs for X-ray analysis were prepared by placing small single crystal seeds of respective polymorphs in contact with a supercooled melt, then heating the melt at various temperatures on a hot stage (SI,

Computational Methods. Density functional theory (DFT) calculations were run in the Gaussian16 software package⁵⁷ using the PBE0 functional⁵⁸ and the 6-311++G(d,p) basis set,^{59,60} as for the optimizations reported in ref 48. The two torsional angles were constrained to fixed values, and all other degrees of freedom were allowed to relax.

Lethality Measurements for IMI Polymorphs. Microcrystals of IMI Forms I, IV, VI, and IX were prepared by grinding respective single crystals using a mortar and pestle (SI, Figure S12). Their compositions were then analyzed by powder X-ray diffraction (PXRD). Lethality measurements were performed in triplicate for each solid-state form, accompanied by three controls (no insecticide). A 2.00 mg portion of microcrystals was added to a 35 mm diameter polystyrene Petri dish that was subsequently shaken to disperse the microcrystals throughout the Petri dish. Microcrystals was added to a polystyrene Petri dish (2.00 mg microcrystals per 35 mm diameter dish for fruit flies; 0.10 mg microcrystals per 100 mm diameter dish for mosquitoes), which was subsequently shaken to disperse the microcrystals throughout the Petri dish. Adult mosquitoes (Ae. aegypti, A. quadrimaculatus, or C. quinquefasciatus) or fruit flies (D. melanogaster) were sedated with carbon dioxide and 30 female mosquitoes or 20 flies were transferred to each Petri dish. The Petri dishes were closed and the motion of the insects was recorded with a video camera (Sony HDR-CX455). The knockdown time was measured for each individual insect, with knockdown associated with an insect laying on the bottom surface of the Petri dish in a supine position without moving from its original position after 10 s.

Statistical Analyses. Logistic regression of knockdown-time curves was preformed to obtain the median knockdown time (KT_{50}) of the test flies and mosquitoes, the 95% confidence intervals (CI), slopes, and standard errors (SE) using Qcal software.

ASSOCIATED CONTENT

Supporting Information

The Supporting Information is available free of charge at https://pubs.acs.org/doi/10.1021/jacs.1c07610.

Experimental details, computational details, preparation and characterization of IMI crystal polymorphs, crystal data, and logistic regression of knockdown-time curves (PDF)

Accession Codes

CCDC 2093848–2093854 contain the supplementary crystallographic data for this paper. These data can be obtained free of charge via www.ccdc.cam.ac.uk/data_request/cif, or by emailing data_request@ccdc.cam.ac.uk, or by contacting The Cambridge Crystallographic Data Centre, 12 Union Road, Cambridge CB2 1EZ, UK; fax: +44 1223 336033.

AUTHOR INFORMATION

Corresponding Authors

Michael D. Ward – Department of Chemistry and Molecular Design Institute, New York University, New York, New York 10003, United States; orcid.org/0000-0002-2090-781X; Email: mdw3@nyu.edu

Bart Kahr — Department of Chemistry and Molecular Design Institute, New York University, New York, New York 10003, United States; Occid.org/0000-0002-7005-4464; Email: bart.kahr@nyu.edu

Authors

Xiaolong Zhu — Department of Chemistry and Molecular Design Institute, New York University, New York, New York 10003, United States; ◎ orcid.org/0000-0003-1511-1566

Chunhua T. Hu — Department of Chemistry and Molecular Design Institute, New York University, New York, New York 10003, United States; Occid.org/0000-0002-8172-2202

Bryan Erriah — Department of Chemistry and Molecular Design Institute, New York University, New York, New York 10003, United States; Occid.org/0000-0003-0608-8069

Leslie Vogt-Maranto — Department of Chemistry, New York University, New York, New York 10003, United States; orcid.org/0000-0002-7006-4582

Jingxiang Yang — Department of Chemistry and Molecular Design Institute, New York University, New York, New York 10003, United States; orcid.org/0000-0002-0859-6668

Yongfan Yang — Department of Chemistry and Molecular Design Institute, New York University, New York, New York 10003, United States; Ocid.org/0000-0003-3511-9733

Mengdi Qiu – Department of Chemistry and Molecular Design Institute, New York University, New York, New York 10003, United States

Noalle Fellah — Department of Chemistry and Molecular Design Institute, New York University, New York, New York 10003, United States

Mark E. Tuckerman — Department of Chemistry and Molecular Design Institute, New York University, New York, New York 10003, United States; Courant Institute of Mathematical Sciences, New York University, New York, New York 10012, United States; NYU-ECNU Center for Computational Chemistry, New York University Shanghai, Shanghai 200062, China; orcid.org/0000-0003-2194-9955

Complete contact information is available at: https://pubs.acs.org/10.1021/jacs.1c07610

Notes

The authors declare the following competing financial interest(s): NYU applied for a provisional patent on new polymorphic forms of imidacloprid.

ACKNOWLEDGMENTS

This work was primarily supported by the New York University Materials Research Science and Engineering Center (MRSEC) program of the National Science Foundation under award number DMR-1420073. It was partially supported by the NSF DMR-1706716. The NYU X-ray facility is supported partially by the NSF under Award Number CRIF/CHE-0840277. Calculations were run on the NYU High Performance Computing clusters.

REFERENCES

- (1) United Nations Sustainable Development Goals. https://sustainabledevelopment.un.org/topics/sustainabledevelopmentgoals (accessed 2021-07-19).
- (2) Oxborough, R. M.; Seyoum, A.; Yihdego, Y.; Dabire, R.; Gnanguenon, V.; Wat'senga, F.; Agossa, F. R.; Yohannes, G.; Coleman, S.; Samdi, L. M.; Diop, A.; Faye, O.; Magesa, S.; Manjurano, A.; Okia, M.; Alyko, E.; Masendu, H.; Baber, I.; Sovi, A.; Rakotoson, J. D.; Varela, K.; Abong'o, B.; Lucas, B.; Fornadel, C.; Dengela, D. Susceptibility testing of Anopheles malaria vector with the neonicotinoid insecticide, clothianidin; results from 16 African countries, in preparation for indoor residual spraying with new insecticide formulations. *Malar. J.* 2019, *18*, 264.
- (3) Kupferschmidt, K. Pick your poison. Science 2016, 354, 171–173.
- (4) Georghiou, G. P.; Mellon, R. B. Pesticide resistance in time and space. In *Pest Resistance to Pesticides*; Georghiou, G. P., Saito, T., Eds.; Springer: 1983; pp 1–46.
- (5) World Health Organization Prequalified Vector Control Products. https://extranet.who.int/pqweb/vector-control-products/prequalified-product-list (accessed 2021-07—19).
- (6) Bhatt, S.; Gething, P. W.; Brady, O. J.; Messina, J. P.; Farlow, A. W.; Moyes, C. L.; Drake, J. M.; Brownstein, J. S.; Hoen, A. G.; Sankoh, O.; Myers, M. F.; George, D. B.; Jaenisch, T.; Wint, G. R.; Simmons, C. P.; Scott, T. W.; Farrar, J. J.; Hay, S. I. The global distribution and burden of Dengue. *Nature* 2013, 496, 504–507.
- (7) World Health Organization. A global brief on vector-borne diseases. World Health Organization, 2014. https://apps.who.int/iris/bitstream/handle/10665/111008/WHO_DCO_WHD_2014.1_eng.pdf?sequence=1&isAllowed=y (accessed 2021-07-19).
- (8) Prequalification Team-Vector Control Group (PQT-VC). Prequalification Team Vector Control Decision Document: Cielo ULV Adulticide Space Spray. World Health Organization, 2019. https://www.who.int/pq-vector-control/prequalified-lists/FinaldecisionCielo.pdf?ua=1 (accessed 2021–07–19).
- (9) Pridgeon, J. W.; Pereira, R. M.; Becnel, J. J.; Allan, S. A.; Clark, G. G.; Linthicum, K. J. Susceptibility of Aedes aegypti, Culex quinquefasciatus Say, and Anopheles quadrimaculatus to 19 pesticides with different modes of action. *J. Med. Entomol.* **2008**, 45, 82–87.
- (10) Buchholz, A.; Nauen, R. Translocation and translaminar bioavailability of two neonicotinoid insecticides after foliar application. *Pest Manage. Sci.* **2002**, *58*, 10–16.
- (11) Weichel, L.; Nauen, R. Uptake, translocation and bioavailability of imidacloprid in several hop varieties. *Pest Manage. Sci.* **2004**, *60*, 440–446.
- (12) Yamamoto, I.; Casida, J. E. Nicotinoid Insecticides and the Nicotinic Acetylcholine Receptor; Springer-Verlag: 1999.
- (13) Sheets, L. P. Chapter 95 Imidacloprid: A Neonicotinoid Insecticide. In *Hayes' Handbook of Pesticide Toxicology*, 3rd ed.; Krieger, R., Ed.; Academic Press: 2010; pp 2055–2064.
- (14) Simon-Delso, N.; Amaral-Rogers, V.; Belzunces, L. P.; Bonmatin, J. M.; Chagnon, M.; Downs, C.; Furlan, L.; Gibbons, D. W.; Giorio, C.; Girolami, V.; Goulson, D.; Kreutzweiser, D. P.; Krupke, C. H.; Liess, M.; Long, E.; McField, M.; Mineau, P.; Mitchell, E. A.; Morrissey, C. A.; Noome, D. A.; Pisa, L.; Settele, J.; Stark, J. D.; Tapparo, A.; Van Dyck, H.; Van Praagh, J.; Van der Sluijs, J. P.; Whitehorn, P. R.; Wiemers, M. Systemic insecticides (neonicotinoids

- and fipronil): trends, uses, mode of action and metabolites. *Environ. Sci. Pollut. Res.* **2015**, 22, 5–34.
- (15) Goulson, D. Review: an overview of the environmental risks posed by neonicotinoid insecticides. *J. Appl. Ecol.* **2013**, *50*, 977–987.
- (16) Morrissey, C. A.; Mineau, P.; Devries, J. H.; Sanchez-Bayo, F.; Liess, M.; Cavallaro, M. C.; Liber, K. Neonicotinoid contamination of global surface waters and associated risk to aquatic invertebrates: a review. *Environ. Int.* **2015**, *74*, 291–303.
- (17) Hallmann, C. A.; Foppen, R. P. B.; van Turnhout, C. A. M.; de Kroon, H.; Jongejans, E. Declines in insectivorous birds are associated with high neonicotinoid concentrations. *Nature* **2014**, *511*, 341–343.
- (18) Eng, M.; Stutchbury, B.; Morrissey, C. A neonicotinoid insecticide reduces fueling and delays migration in songbirds. *Science* **2019**, *365*, 1177–1180.
- (19) van Klink, R.; Bowler, D. E.; Gongalsky, K. B.; Swengel, A. B.; Gentile, A.; Chase, J. M. Meta-analysis reveals declines in terrestrial but increases in freshwater insect abundances. *Science* **2020**, *368*, 417–420.
- (20) Basset, Y.; Lamarre, G. P. Toward a world that values insects. *Science* **2019**, *364*, 1230–1231.
- (21) Whitehorn, P. R.; O'Connor, S.; Wackers, F. L.; Goulson, D. Neonicotinoid pesticide reduces bumble bee colony growth and queen production. *Science* **2012**, *336*, 351–352.
- (22) Kessler, S.; Tiedeken, E. J.; Simcock, K. L.; Derveau, S.; Mitchell, J.; Softley, S.; Stout, J. C.; Wright, G. A. Bees prefer foods containing neonicotinoid pesticides. *Nature* **2015**, *521*, 74–76.
- (23) Stanley, D. A.; Garratt, M. P.; Wickens, J. B.; Wickens, V. J.; Potts, S. G.; Raine, N. E. Neonicotinoid pesticide exposure impairs crop pollination services provided by bumblebees. *Nature* **2015**, *528*, 548–550.
- (24) Crall, J. D.; Switzer, C. M.; Oppenheimer, R. L.; Ford Versypt, A. N.; Dey, B.; Brown, A.; Eyster, M.; Guérin, C.; Pierce, N. E.; Combes, S. A.; de Bivort, B. L. Neonicotinoid exposure disrupts bumblebee nest behavior, social networks, and thermoregulation. *Science* 2018, 362, 683–686.
- (25) Sánchez-Bayo, F.; Goulson, D.; Pennacchio, F.; Nazzi, F.; Goka, K.; Desneux, N. Are bee diseases linked to pesticides? A brief review. *Environ. Int.* **2016**, *89*, 7–11.
- (26) Biodiversity Act, 2016. Law no. 2016–1087, 8 August 2016, For the return of biodiversity, nature, and countryside. https://www.legifrance.gouv.fr/eli/loi/2016/8/8/2016-1087/jo/texte (accessed 2021–07–19).].
- (27) Pretty, J.; Bharucha, Z. P. Integrated Pest Management for sustainable intensification of agriculture in Asia and Africa. *Insects* **2015**, *6*, 152–182.
- (28) Dzul-Manzanilla, F.; Correa-Morales, F.; Medina-Barreiro, A.; Bibiano-Marín, W.; Vadillo-Sanchez, J.; Riestra-Morales, M.; Del Castillo-Centeno, L. F.; Morales-Rios, E.; Martin-Park, A.; Gonzalez-Olvera, G.; Elizondo-Quiroga, A. E.; Lenhart, A.; Vazquez-Prokopec, G.; Che-Mendoza, A.; Manrique-Saide, P. Field efficacy trials of aerial ultra-low-volume application of insecticides against caged Aedes aegypti in Mexico. *J. Am. Mosq. Control Assoc.* 2019, 35, 140–146.
- (29) Yang, J.; Hu, C. T.; Zhu, X.; Zhu, Q.; Ward, M. D.; Kahr, B. DDT Polymorphism and the Lethality of Crystal Forms. *Angew. Chem., Int. Ed.* **2017**, *56*, 10165–10169.
- (30) Yang, J.; Zhu, X.; Hu, C. T.; Qiu, M.; Zhu, Q.; Ward, M. D.; Kahr, B. Inverse Correlation between Lethality and Thermodynamic Stability of Contact Insecticide Polymorphs. *Cryst. Growth Des.* **2019**, 19, 1839–1844.
- (31) Zhu, X.; Hu, C. T.; Yang, J.; Joyce, L. A.; Qiu, M.; Ward, M. D.; Kahr, B. Manipulating solid forms of contact insecticides for infectious disease prevention. *J. Am. Chem. Soc.* **2019**, *141*, 16858–16864.
- (32) Yang, J.; Erriah, B.; Hu, C. T.; Reiter, E.; Zhu, X.; López-Mejías, V.; Carmona-Sepúlveda, I. P.; Ward, M. D.; Kahr, B. A deltamethrin crystal polymorph for more effective malaria control. *Proc. Natl. Acad. Sci. U. S. A.* **2020**, *117*, 26633–26638.
- (33) Le Questel, J.-Y.; Graton, J.; Cerón-Carrasco, J. P.; Jacquemin, D.; Planchat, A.; Thany, S. H. New insights on the molecular features and electrophysiological properties of dinotefuran, imidacloprid and

- acetamipid neonicotinoid insecticides. *Bioorg. Med. Chem.* **2011**, *19*, 7623–7634.
- (34) Zhao, J.; Wang, M.; Dong, B.; Feng, Q.; Xu, C. Monitoring the polymorphic transformation of imidacloprid using in situ FBRM and PVM. *Org. Process Res. Dev.* **2013**, *17*, 375–381.
- (35) Kagabu, S.; Matsuno, H. Chloronicotinyl insecticides. 8. Crystal and molecular structures of imidacloprid and analogous compounds. *J. Agric. Food Chem.* **1997**, *45*, 276–281.
- (36) Chopra, D.; Mohan, T. P.; Rao, K. S.; Row, T. N. G. (2E)-1-[(6-Chloropyridin-3-yl)methyl]-N-nitro-imidazolidin-2-imine (imidachloprid). *Acta Crystallogr., Sect. E: Struct. Rep. Online* **2004**, *60*, No. 02415-02417.
- (37) Xue, S.; Xu, J.; Han, Y.; Zhang, J.; Li, W. Solvent-antisolvent competitive interactions mediate imidacloprid polymorphs in antisolvent crystallization. *Cryst. Growth Des.* **2021**, *21*, 4318–4328.
- (38) Zhu, Q.; Shtukenberg, A. G.; Carter, D. J.; Yu, T. Q.; Yang, J.; Chen, M.; Raiteri, P.; Oganov, A. R.; Pokroy, B.; Polishchuk, I.; Bygrave, P. J.; Day, G. M.; Rohl, A. L.; Tuckerman, M. E.; Kahr, B. Resorcinol crystallization from the melt: A new ambient phase, and new 'riddles'. *J. Am. Chem. Soc.* **2016**, *138*, 4881–4889.
- (39) Shtukenberg, A. G.; Zhu, Q.; Carter, D. J.; Vogt, L.; Hoja, J.; Schneider, E.; Song, H.; Pokroy, B.; Polishchuk, I.; Tkatchenko, A.; Oganov, A. R.; Rohl, A. L.; Tuckerman, M. E.; Kahr, B. Powder diffraction and crystal structure prediction reveal four new coumarin polymorphs. *Chem. Sci.* **2017**, *8*, 4926–4940.
- (40) Shtukenberg, A. G.; Punin, Y. O.; Gunn, E.; Kahr, B. Spherulites. *Chem. Rev.* **2012**, *112*, 1805–1838.
- (41) Cui, X.; Rohl, A. L.; Shtukenberg, A. G.; Kahr, B. Twisted aspirin crystals. J. Am. Chem. Soc. 2013, 135, 3395–3398.
- (42) Shtukenberg, A. G.; Zhu, X.; Yang, Y.; Kahr, B. Common occurrence of twisted molecular crystal morphologies from the melt. *Cryst. Growth Des.* **2020**, *20*, 6186–6197.
- (43) Mitchell, C. A.; Yu, L.; Ward, M. D. Selective nucleation and discovery of organic polymorphs through epitaxy with single crystal substrates. *J. Am. Chem. Soc.* **2001**, *123*, 10830–10839.
- (44) Yu, L. Nucleation of one polymorph by another. *J. Am. Chem. Soc.* **2003**, *125*, 6380–6381.
- (45) Chen, S.; Xi, H.; Yu, L. Cross-nucleation between ROY polymorphs. J. Am. Chem. Soc. 2005, 127, 17439–17444.
- (46) Ha, J.-M.; Wolf, J. H.; Hillmyer, M. A.; Ward, M. D. Polymorph selectivity under nanoscopic confinement. *J. Am. Chem. Soc.* **2004**, 126, 3382–3383.
- (47) Moreira, A. A. G.; De Lima-Neto, P.; Caetano, E. W. S.; Barroso-Neto, I. L.; Freire, V. N. Computational electronic structure of the bee killer insecticide imidacloprid. *New J. Chem.* **2016**, *40*, 10353–10362.
- (48) García-Hernández, E.; Flores-Moreno, R.; Vázquez-Mayagoitia, Á.; Vargas, R.; Garza, J. Initial stage of the degradation of three common neonicotinoids: theoretical prediction of charge transfer sites. *New J. Chem.* **2017**, *41*, 965–974.
- (49) Schneider, D. Using Drosophila as a model Insect. *Nat. Rev. Genet.* **2000**, *1*, 218–226.
- (50) Lozano-Fuentes, S.; Saavedra-Rodriguez, K.; Black, W. C.; Eisen, L. QCal: A software application for the calculation of doseresponse curves in insecticide resistance bioassays. *J. Am. Mosq. Control Assoc.* **2012**, *28*, 59–61.
- (51) Grubaugh, N. D.; Ladner, J. T.; Kraemer, M. U. G.; Dudas, G.; Tan, A. L.; Gangavarapu, K.; Wiley, M. R.; White, S.; Thezé, J.; Magnani, D. M.; Prieto, K.; Reyes, D.; Bingham, A. M.; Paul, L. M.; Robles-Sikisaka, R.; Oliveira, G.; Pronty, D.; Barcellona, C. M.; Metsky, H. C.; Baniecki, M. L.; Barnes, K. G.; Chak, B.; Freije, C. A.; Gladden-Young, A.; Gnirke, A.; Luo, C.; Maclnnis, B.; Matranga, C. B.; Part, D. J.; Schaffner, S. F.; Tomkins-Tinch, C.; West, K. L.; Winnicki, D. I.; Cone, M. R.; Kopp, E. W., IV; Hogan, K. N.; Cannons, A. C.; Jean, R.; Monaghan, A. J.; Garry, R. F.; Loman, N. J.; Faria, N. R.; Porcelli, M. C.; Vasquez, C.; Nagle, E. R.; Cummings, D. A. T.; Stanek, D.; Rambaut, A.; Sanchez-Lockhart, M.; Sabeti, P. C.; Gillis, L. D.; Michael, S. F.; Bedford, T.; Pybus, O. G.; Isern, S.; Palacios, G.; Andersen, K. G.; et al. Genomic epidemiology reveals

multiple introductions of Zika virus into the United States. *Nature* **2017**, *546*, 401–405.

- (52) Metsky, H. C.; Matranga, C. B.; Wohl, S.; Schaffner, S. F.; Freije, C. A.; Winnicki, S. M.; West, K.; Qu, J.; Baniecki, M. L.; Gladden-Young, A.; Lin, A. E.; Tomkins-Tinch, C. H.; Ye, S. H.; Park, D. J.; Luo, C. Y.; Barnes, K. G.; Shah, R. R.; Chak, B.; Barbosa-Lima, G.; Delatorre, E.; Vieira, Y. R.; Paul, L. M.; Tan, A. L.; Barcellona, C. M.; Porcelli, M. C.; Vasquez, C.; Cannons, A. C.; Cone, M. R.; Hogan, K. N.; Kopp, E. W.; Anzinger, J. J.; Garcia, K. F.; Parham, L. A.; Ramírez, R. M. G.; Montoya, M. C. M.; Rojas, D. P.; Brown, C. M.; Hennigan, S.; Sabina, B.; Scotland, S.; Gangavarapu, K.; Grubaugh, N. D.; Oliveira, G.; Robles-Sikisaka, R.; Rambaut, A.; Gehrke, L.; Smole, S.; Halloran, M. E.; Villar, L.; Mattar, S.; Lorenzana, I.; Cerbino-Neto, J.; Valim, C.; Degrave, W.; Bozza, P. T.; Gnirke, A.; Andersen, K. G.; Isern, S.; Michael, S. F.; Bozza, F. A.; Souza, T. M. L.; Bosch, I.; Yozwiak, N. L.; MacInnis, B. L.; Sabeti, P. C. Zika virus evolution and spread in the Americas. *Nature* 2017, 546, 411–415.
- (53) Barrett, A. D. T. The reemergence of yellow fever. *Science* **2018**, *361*, 847–848.
- (54) Smol, J. P. Climate change: a planet in flux. *Nature* **2012**, *483*, S12–S15.
- (55) Makoni, M. Malaria fighters' latest chemical weapon may not last long. *Science* **2020**, *369*, 1153.
- (56) Riaz, M. A.; Chandor-Proust, A.; Dauphin-Villemant, C.; Poupardin, R.; Jones, C. M.; Strode, C.; Régent-Kloeckner, M.; David, J. P.; Reynaud, S. Molecular mechanisms associated with increased tolerance to the neonicotinoid insecticide imidacloprid in the dengue vector Aedes aegypti. *Aquat. Toxicol.* **2013**, *126*, 326–337.
- (57) Frisch, M. J.; Trucks, G. W.; Schlegel, H. B.; Scuseria, G. E.; Robb, M. A.; Cheeseman, J. R.; Scalmani, G.; Barone, V.; Petersson, G. A.; Nakatsuji, H.; Li, X.; Caricato, M.; Marenich, A. V.; Bloino, J.; Janesko, B. G.; Gomperts, R.; Mennucci, B.; Hratchian, H. P.; Ortiz, J. V.; Izmaylov, A. F.; Sonnenberg, J. L.; Williams-Young, D.; Ding, F.; Lipparini, F.; Egidi, F.; Goings, J.; Peng, B.; Petrone, A.; Henderson, T.; Ranasinghe, D.; Zakrzewski, V. G.; Gao, J.; Rega, N.; Zheng, G.; Liang, W.; Hada, M.; Ehara, M.; Toyota, K.; Fukuda, R.; Hasegawa, J.; Ishida, M.; Nakajima, T.; Honda, Y.; Kitao, O.; Nakai, H.; Vreven, T.; Throssell, K.; Montgomery, J. A., Jr.; Peralta, J. E.; Ogliaro, F.; Bearpark, M. J.; Heyd, J. J.; Brothers, E. N.; Kudin, K. N.; Staroverov, V. N.; Keith, T. A.; Kobayashi, R.; Normand, J.; Raghavachari, K.; Rendell, A. P.; Burant, J. C.; Iyengar, S. S.; Tomasi, J.; Cossi, M.; Millam, J. M.; Klene, M.; Adamo, C.; Cammi, R.; Ochterski, J. W.; Martin, R. L.; Morokuma, K.; Farkas, O.; Foresman, J. B.; Fox, D. J.; Gaussian 16, Revision A.03; Gaussian Inc.: Wallingford, CT, 2016.
- (58) Adamo, C.; Barone, V. Toward reliable density functional methods without adjustable parameters: The PBE0 model. *J. Chem. Phys.* **1999**, *110*, 6158–6169.
- (59) Hehre, W. J.; Ditchfield, R.; Pople, J. A. Self-consistent molecular orbital methods. XII. Further extensions of Gaussian-type basis sets for use in molecular-orbital studies of organic-molecules. *J. Chem. Phys.* **1972**, *56*, 2257.
- (60) Frisch, M. J.; Pople, J. A.; Binkley, J. S. Self-consistent molecular orbital methods. 25. Supplementary functions for Gaussian basis sets. *J. Chem. Phys.* **1984**, *80*, 3265–3269.